Solar Energy Materials & Solar Cells 159 (2017) 265–271

Contents lists available at ScienceDirect

Solar Energy Materials & Solar Cells

journal homepage: www.elsevier.com/locate/solmat

The application of poly-Si/SiO_x contacts as passivated top/rear contacts in Si solar cells

Frank Feldmann [a,b,*], Christian Reichel [a], Ralph Müller [a,b], Martin Hermle [a]

[a] Fraunhofer ISE, Heidenhofstr. 2, D-79110 Freiburg, Germany
[b] Albert Ludwig University Freiburg, Department of Sustainable Systems Engineering, Georges-Köhler-Allee 103, D-79110 Freiburg, Germany

ARTICLE INFO

Article history:
Received 21 April 2016
Received in revised form
30 June 2016
Accepted 12 September 2016
Available online 23 September 2016

Keywords:
Passivated contact
Poly-Si contacts
Tunnel oxide
Surface passivation

ABSTRACT

Passivated contacts based on low-pressure chemical vapor deposited (LPCVD) heavily-doped poly-Si and a thin SiO_x layer are explored for the application in an interdigitated back contact (IBC) solar cell. The poly-Si/SiO_x contacts are realized by applying wet-chemically grown SiO_x tunnel layers and amorphous Si (a-Si) layers doped via ion implantation that are subsequently transformed into poly-Si/SiO_x contacts by a high temperature step. The impact of doping species, ion dose, and poly-Si thickness on the surface passivation of such contacts is studied. Excellent J_0 values down to 4.5 fA/cm^2 were measured for n^+-poly-Si contacts, while J_0 values as low as 22 fA/cm^2 were obtained for p^+-poly-Si contacts. Solar cells with top/rear poly-Si contacts were processed and V_{oc} values up to 709 mV and *FF* values above 81% were measured. Furthermore, the upper bound for the parasitic absorption losses in 10–40 nm thick poly-Si films was quantified to be about 0.5 mA/cm^2 per 10 nm poly-Si layer thickness.

1. Introduction

Carrier-selective contacts have pushed the efficiency of crystalline silicon (c-Si) solar cells notably in the past few years. The most well-known concept is the heterojunction solar cell, where hydrogenated amorphous silicon (a-Si:H) layers enable very low surface recombination velocities and outstanding V_{oc} values up to 750 mV [1]. Another promising concept – often referred to as passivated contact – makes use of a stack of an ultra-thin SiO_x layer and a heavily doped silicon film (e.g. poly-Si, SIPOS [2], or TOPCon [3]). The realization of an n-type solar cell with boron diffused front and passivated contact (TOPCon) at the rear led to an efficiency of 25.1% [4], which shares the world record for a solar cell featuring top/rear contacts with a large area heterojunction solar cell reported in [5]. Since all silicon based carrier-selective contacts cause significant parasitic absorption losses in the blue wavelength range, it is instructive to place both polarities of the carrier-selective contacts exclusively at the rear side. As a result, the implementation of the a-Si/c-Si heterojunction into an interdigitated back contact (IBC) solar cell design even led to the world record efficiency of 25.6% for Si solar cells [6]. The fabrication of such solar cells, however, involves complex patterning steps. On the other hand, the use of poly-Si layers in combination with masked ion implantation could simplify the fabrication of IBC solar cells. Ion implantation has already been used to form passivated contacts in IBC silicon solar cells or precursors [7–11]. These approaches were either based on semi-crystalline silicon films (TOPCon) or on more than a 100 nm thick polycrystalline silicon films.

This paper addresses solar cells with poly-Si/SiO_x contacts on both sides. To reduce the parasitic absorption in these contacts, thin poly-Si layers between 10 nm and 40 nm were investigated. The poly-crystalline silicon films were realized by LPCVD (low-pressure chemical vapor deposited) a-Si layers, doping using ion implantation and subsequent crystallization. To this end, symmetrical lifetime samples and both-sides contacted solar cells were fabricated to determine the passivation quality and the junction characteristics of these poly-Si/SiO_x contacts as a function of their thickness. Moreover, parasitic absorption losses in the poly-Si contacts were quantified.

2. Experimental details

Symmetrical lifetime samples were prepared on 200 μm thick, shiny-etched n-type 1 Ω cm FZ Si wafers. The wafers were cleaned according to the RCA cleaning procedure. After the final HF dip, the wafers were immersed in boiling nitric acid (68 wt%, 120 °C) thereby growing a thin tunnel oxide layer. The wafers were then loaded into an LPCVD reactor and undoped a-Si was deposited at 485 °C. The a-Si thickness was varied between nominal 10, 20, and 40 nm. In addition, 40 nm a-Si was deposited on oxidized wafers (~100 nm SiO_2) for optical characterization. Thereafter, low energy ion implantation was used to form the doped poly-Si contacts. Phosphorus (P) was

* Corresponding author.
E-mail address: frank.feldmann@ise.fraunhofer.de (F. Feldmann).

http://dx.doi.org/10.1016/j.solmat.2016.09.015
0927-0248/

implanted at 2 keV with ion doses ranging from 1×10^{14} cm^{-2} to 2.5×10^{15} cm^{-2} to form electron-selective contacts. Hole selective contacts were realized by either implanting boron (B) at 1 keV or boron-monofluoride (BF) at 2 keV with ion doses ranging from 1×10^{14} to 1×10^{15} cm^{-2}. After ion implantation the wafers received a 10-min anneal in a tube furnace (N_2 atmosphere) at 850 °C and 875 °C, respectively. To further improve the surface passivation, the samples were subjected to a remote plasma hydrogen passivation process (RPHP) at 400 °C for 30 min [12].

The surface passivation quality was measured after furnace annealing and hydrogen passivation using a Sinton WCT-120 lifetime tester [13]. Here, the implied open-circuit voltage (iV_{oc}) at one sun is given as a means to assess the surface passivation quality. Furthermore, the P or B atoms that diffused from the poly-Si layer into the c-Si were measured by electrochemical capacitance-voltage (ECV) profiling starting on the poly-Si film.

Simple 2×2 cm^2 sized planar solar cells were prepared in order to assess the carrier selectivity of both poly-Si contacts. The solar cell structure is shown in Fig. 1. The absorber is a 250 μm thick p-type 1 Ω cm FZ Si wafer. To this end, the n^+-poly-Si and p^+-poly-Si contacts were realized on the front and rear, respectively, in a similar fashion as described above. The ion dose was 1×10^{15} cm^{-2} and the furnace anneal was 850 °C for 10 min. Since the thin poly-Si films have a sheet resistance in the order of 1000 Ω/sq, a transparent conductive oxide (TCO) stack was deposited on the front through a 2.2×2.2 cm^2 shadow mask to provide for sufficient lateral conductivity and reduce the front surface reflection. The stack consisted of a 20 nm thick atomic layer deposited Al-doped zinc oxide (AZO) interlayer and 55 nm sputtered indium tin oxide (ITO) providing a low sheet resistance of 125 ± 10 Ω/sq and enabling good contact to n^+-poly-Si while avoiding sputter damage (see Ref. [14] for more details). The front grid featuring 60 μm wide and 2.5 μm high fingers was realized by thermal evaporation of Ti/Pd/Ag and the lift-off technique. The rear side was fully covered with thermally evaporated Ag.

The SunsVoc characteristics of the finished solar cells were taken using a Sinton SunsVoc tester [15] and the light *J-V* characteristics were recorded using a sun simulator calibrated to a Fraunhofer ISE reference cell. The series resistance of the cells was determined by comparing SunsVoc and light *J-V* curve [16]. Moreover, the external quantum efficiency and reflection curve were measured.

3. Film thickness and optical properties of poly-Si

The quantitative assessment of parasitic absorption losses in poly-Si demands good confidence in the poly-Si film thickness and its optical properties. The film thickness after deposition, and thus deposition rate, as well as the film thickness after the furnace anneal were determined by spectroscopic ellipsometry (SE) and scanning electron beam microscopy (SEM) on a reference wafer having a ~100 nm thick thermally-grown SiO_2 film underneath the a-Si/poly-Si film. The SE data of the nominal 40 nm thick a-Si film was fitted with a Tauc-Lorentz oscillator [17] and yielded $t_{a\text{-}Si} = 37.2$ nm and $E_{g,\ a\text{-}Si} = 1.43$ eV, which is in good agreement with the estimated thickness obtained from an SEM image of the same sample. The surface roughness was less than 1 nm. The calculated deposition rate of ~0.37 nm/min yielded initial a-Si thicknesses of about 9, 18, and 37 nm for the nominal 10, 20, and 40 nm thick films. Two sets of samples were then doped by ion implantation with BF (1×10^{15} cm^{-2}) and P (1×10^{15} cm^{-2}), respectively. The samples received a furnace anneal at 850 °C and the oxide that grew unintentionally during the furnace anneal was removed in diluted HF. An effective medium approximation (EMA) [18] model consisting of a mixture of undoped poly-Si (small grain size) and arsenic (As)-doped poly-Si (large grain size) (n and k data from Ref. [19]) fitted well the measured SE data and yielded $t_{poly\text{-}Si} \approx 34$ nm and a surface roughness smaller than 2 nm. Thus, about 3 nm of the film was consumed upon furnace annealing. For the thinner films 3 nm consumption of poly-Si was assumed as an upper bound which gives a minimum thickness of about 6 nm and 15 nm for the nominal 10 and 20 nm thin films, respectively.

Modeling of the SE data yielded a slightly different ratio of small and large grain size poly-Si for the differently doped films. The BF-doped and intrinsic poly-Si films were best described by a mixture of 74% large grain size poly-Si and 26% small grain size poly-Si, while the P-doped poly-Si films yielded a mixture of 84% large grain size poly-Si and 16% small grain size poly-Si. Therefore, the average grain size of P-doped poly-Si seems to be somewhat larger than the average grain size of undoped and BF-doped poly-Si. This agrees with literature, where grain growth enhancement was reported for P or As-doped poly-Si, while B had little effect on grain growth [20]. Please note that the terms small and large grain size were not quantitatively defined in Ref. [19]. Therefore, the quantification of the average grain sizes demands further studies using characterization techniques such as x-ray diffraction (XRD), electron backscatter diffraction (EBSD), or transmission electron microscopy (TEM).

The absorption coefficients of the respective films that were determined by SE are plotted in Fig. 2. In addition, the reference values and α of an a-Si:H(i) film described by a Tauc-Lorentz oscillator are given. Although the latter model does not account for sub-bandgap absorption in a-Si:H, one can clearly see that a-Si:H absorbs light more strongly in the relevant energy regime than poly-Si. The higher absorption of the poly-Si films at energies above 3.3 eV is due to the direct bandgap of c-Si at 3.32 eV. Moreover, the poly-Si films have a higher absorption coefficient below the direct bandgap than c-Si as already reported in Ref. [19].

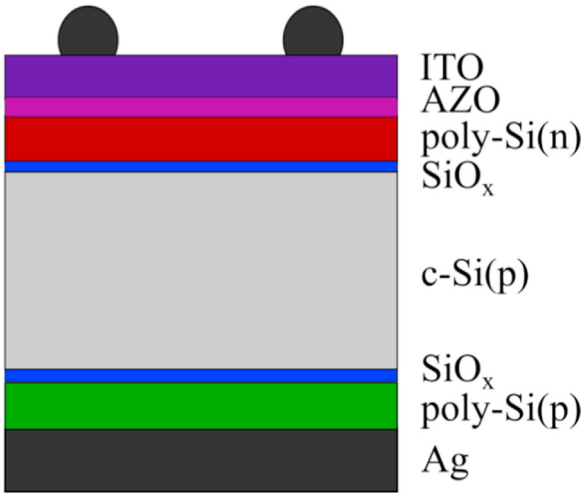

Fig. 1. Sketch of solar cell design.

4. Surface passivation of poly-Si contacts

4.1. Phosphorus-doped poly-Si contacts

Fig. 3 depicts the mean iV_{oc} obtained on samples passivated with n^+-poly-Si contacts formed by ion implantation. The samples were measured after annealing (open symbols) and after hydrogen passivation by RPHP (closed symbols). The left figure depicts the iV_{oc} obtained from 15 nm thick n^+-poly-Si contacts featuring different ion doses. The lowest dose of 1×10^{14} cm^{-2} did not produce a reasonable surface passivation before and after hydrogen passivation. It is concluded that the dose was too low to sufficiently dope the poly-Si. With increasing dose the surface passivation measured after annealing improved up to 700 mV for a dose of 1×10^{15} cm^{-2}

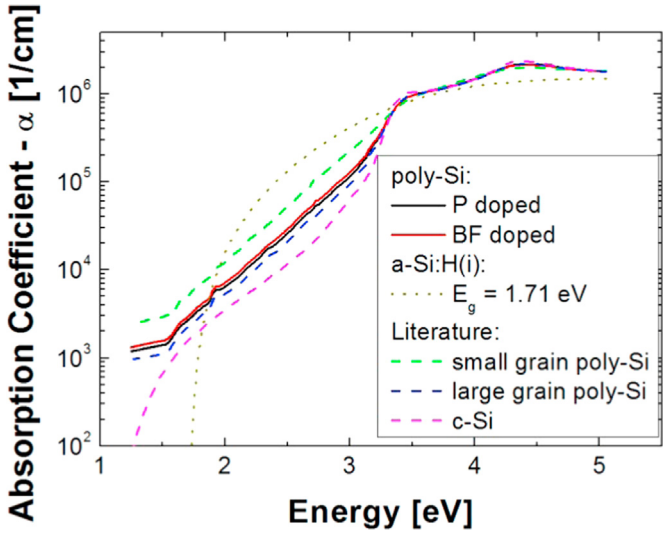

Fig. 2. Absorption coefficients of P-doped and BF-doped poly-Si films determined by fitting the SE data with an EMA model of small and large grain size poly-Si. The reference data from Ref. [15] are also given as well as the absorption coefficient of intrinsic a-Si:H determined by the Tauc-Lorentz oscillator.

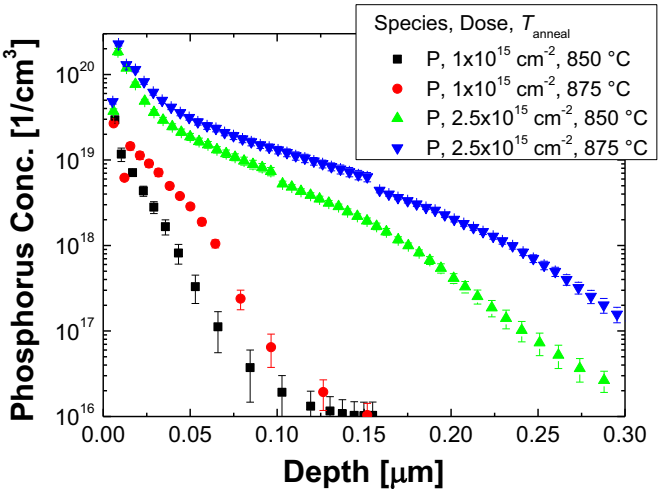

Fig. 4. Phosphorus profile obtained on 15 nm thick poly-Si contacts with different doping doses and annealing temperatures. The ECV measurement started on the poly-Si film and extended into the silicon substrate.

and then dropped sharply to about 670 mV for a dose of 2.5×10^{15} cm^{-2}. After hydrogen passivation the iV_{oc} improved markedly up to 720 mV for a dose of 1×10^{15} cm^{-2}, while the iV_{oc} of the samples featuring a very high dose of 2.5×10^{15} cm^{-2} did not improve. Moreover, it can be seen that the higher annealing temperature of 875 °C always led to lower iV_{oc} values. It was inferred from this experiment that the optimum doping dose is about 1×10^{15} cm^{-2} and was then kept constant for the next experiment presented in Fig. 3 (right). Here, the poly-Si thickness was ~6 nm, 15 nm, and 34 nm. Again, it was found that the higher annealing temperature yielded lower iV_{oc} values than the 850 °C anneal. The iV_{oc} value after annealing (open symbols) first increased with poly-Si thickness from 708 mV to 714 mV and then decreased for the thickest poly-Si film down to 691 mV. After hydrogen passivation the iV_{oc} values increased significantly and the iV_{oc} increased with poly-Si thickness from 715 mV (6 nm poly-Si) to 733 mV (34 nm poly-Si). The surface passivation of the latter samples was close to the Auger limit of the wafer and a recombination current density (J_0) of ~4.5 fA/cm² was extracted by the Kane & Swanson method [21].

Fig. 4 shows the phosphorus profiles obtained from ECV profiling. It can be clearly seen that the highest ion dose leads to excessive diffusion of phosphorus from the poly-Si into the c-Si during annealing. For a dose of 2.5×10^{15} cm^{-2}, an about 300 nm deep P profile with a surface carrier concentration (N_{surf}) of more than 2×10^{20} cm^{-3} was obtained. The doping profile was then analyzed by the computer program EDNA [22]. A sheet resistance of 110 Ω/sq. was calculated. In addition, the Auger recombination current ($J_{0,\ Auger}$) in the doped c-Si region was calculated by assuming zero surface recombination velocity. $J_{0,\ Auger}$ was about 20 fA/cm² and can only partially account for the low iV_{oc} value of 670 mV. Another reason for the reduced surface passivation could be a fairly high recombination velocity at the SiO_x/c-Si interface, which is caused by the high concentration of charge carriers at the interface and possibly by the large amount of dopants diffused through the SiO_x tunnel layer. At the intermediate doping level of 1×10^{15} cm^{-2}, shallow doping profiles with a depth of about 100 nm and $N_{surf} \ll 1 \times 10^{20}$ cm^{-3} were obtained for both annealing temperatures. $J_{0,\ Auger}$ of both profiles were negligibly small, i.e. below 1 fA/cm^2. As already observed in Ref. [8,23], the surface passivation is not decisively affected by Auger recombination in the heavily-doped c-Si region but seems to rather

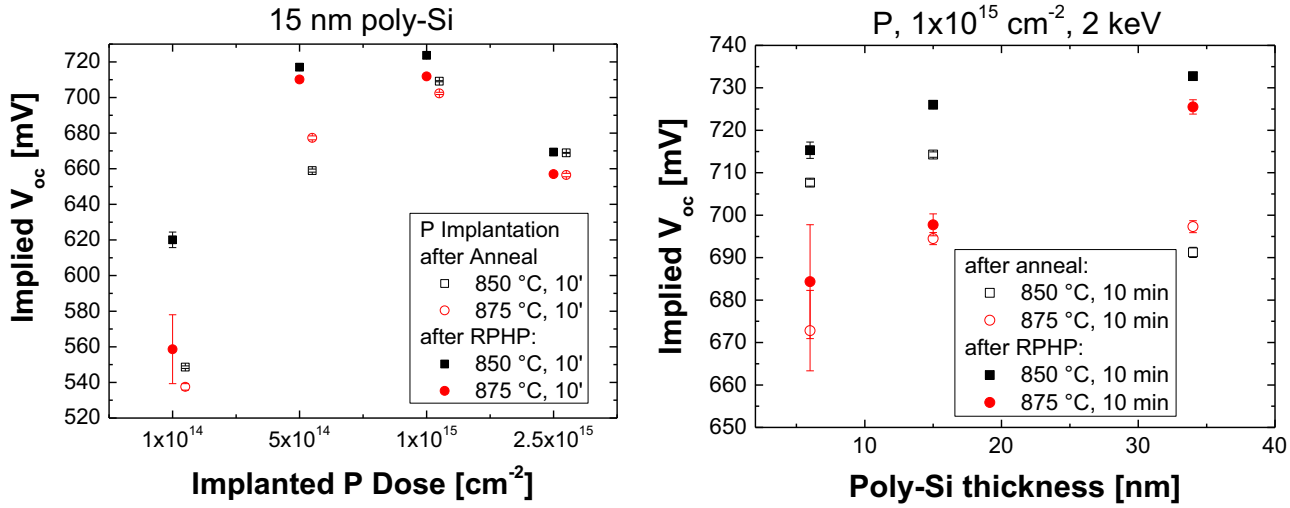

Fig. 3. Implied V_{oc} of n$^+$-poly-Si contacts as a function of ion dose with a fixed poly-Si thickness of 15 nm (left: the open symbols are placed adjacently for clarity) and as a function of poly-Si thickness using a constant ion dose of 1×10^{15} cm^{-2} (right). Each data point represents the mean value of six samples and the error bars refer to the standard error of the mean.

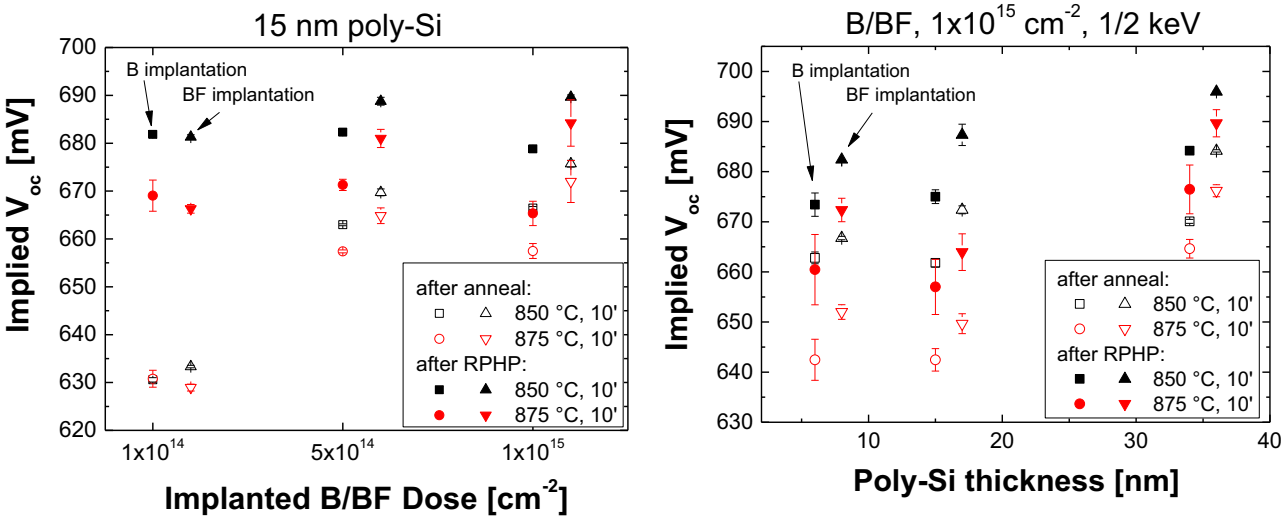

Fig. 5. Implied V_{oc} of p^+-poly-Si contacts as a function of ion dose with a fixed poly-Si thickness of 15 nm (left) and as a function of poly-Si thickness using a constant ion dose of 1×10^{15} cm^{-2} (right). The implanted species was either B (1 keV) or BF (2 keV). The data points corresponding to the latter are placed adjacently for clarity. Each data point represents the mean value of six samples and the error bars refer to the standard error of the mean.

depend on the surface concentration or the amount of P atoms penetrating the oxide.

4.2. Boron-doped poly-Si contacts

Fig. 5 shows the mean iV_{oc} values obtained from p^+-poly-Si contacts formed by ion implantation of B (squares and circles) and BF (up and down-facing triangles), respectively. The doping species BF_2 was not considered here because initial tests as well as tests on TOPCon structures [9] revealed very high contact resistivities. The left graph shows the results of a dose variation between 1×10^{14} cm^{-2} and 1×10^{15} cm^{-2} on 15 nm thick poly-Si contacts. The iV_{oc} values measured after annealing were very low (630 mV) for the lowest dose of 1×10^{14} cm^{-2} and increased up to 676 mV for a dose of 1×10^{15} cm^{-2} (BF implantation). Moreover, the BF implanted samples showed a slightly superior surface passivation than the samples implanted solely with B. This trend kept up after hydrogen passivation upon which the lightly doped samples (dose$=1 \times 10^{14}$ cm^{-2}) improved up to 680 mV and the heavily-doped samples improved up to 690 mV. On average, a gain of about +10 mV was achieved when implanting BF instead of B. For the next experiment shown in Fig. 5 (right), a constant ion dose of 1×10^{15} cm^{-2} was chosen and the poly-Si thickness was varied between 6 nm and 34 nm. Again, slightly higher iV_{oc} values were obtained with BF implantation. Unlike for the n^+-poly-Si contact the surface passivation did not improve significantly with p^+-poly-Si thickness. Nevertheless, the highest iV_{oc} values of 696 mV were obtained for the 34 nm thick, BF implanted poly-Si contacts. This corresponds to a measured J_0 of ~22 fA/cm², which is five times higher than the J_0 obtained from an n^+-poly-Si contact.

The corresponding boron diffusion profiles are depicted in Fig. 6. The profiles are very shallow and their surface concentration was in the range of $1-3 \times 10^{19}$ cm^{-3}. EDNA calculations reveal that Auger recombination (about 1 fA/cm^2) in these regions can be neglected. Hence, the distinct difference in surface passivation between n-type and p-type poly-Si contacts cannot be attributed to Auger recombination but can be rather ascribed with a pronounced increase in the recombination velocity at the interface between p-type poly-Si and c-Si and in the poly-Si layer itself as suggested in Refs. [8,24].

4.3. Discussion

Two main experiments were conducted to determine a suitable parameter set to form n-type and p-type poly-Si/SiO_x contacts with excellent surface passivation. These two experiments were (i) a variation of the dopant dose for a constant poly-Si thickness and (ii) a variation of poly-Si thickness for a constant doping dose.

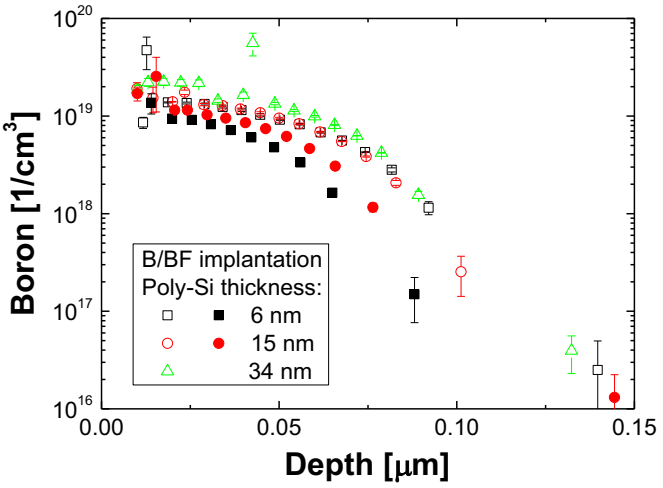

Fig. 6. Boron profile obtained on B (open symbols) and BF (closed symbols) implanted poly-Si contacts having a thickness of ~6 nm, 15 nm, and 34 nm, respectively. The ECV measurement started on the poly-Si film.

For the n^+-poly-Si contacts, it was found that the doping level strongly determines the surface passivation quality after furnace annealing. Too low doping levels produced a weak surface passivation, while too high doping levels led to excessive phosphorus diffusion into the c-Si and lowered the level of surface passivation significantly. Hence, both the furnace anneal and doping level in the poly-Si are to be optimized to produce a very shallow dopant profile within the c-Si, which reduces the number of minority charge carriers at the c-Si/SiO_x interface but does not give rise to a strong contribution from Auger recombination. This relationship between minority carrier recombination and doping level/annealing temperature was also observed by Patton et al. who studied the recombination current of 400 nm thick, As doped poly-Si contacts without deliberately grown tunnel oxide [25]. Furthermore, the role of phosphorus agglomeration at both the poly-Si/SiO_x and SiO_x/c-Si interfaces is not fully understood yet. Neugroschel et al. gave experimental evidence that an agglomeration of dopants at the poly-Si/

c-Si interface is crucial to effectively reduce minority carrier recombination at that interface [26]. This fact also explains why the samples passivated with 15 nm poly-Si contacts yielded markedly higher iV_{oc} values (714 mV) than those with 34 nm poly-Si contacts (691 mV) after annealing at 850 °C. The reason is that in the latter case the phosphorus atoms were implanted further away from the interface and a fewer number of dopants diffused to that interface during the high-temperature anneal. Therefore, the higher annealing temperature of 875 °C led to a slight increase in surface passivation, while it otherwise led to a decrease in surface passivation. Furthermore, the hydrogen passivation proved to be very effective for the 15 nm and 34 nm thick poly-Si contacts and the highest iV_{oc} value of 733 mV was obtained for the 34 nm thick poly-Si contact.

For the realization of p-type poly-Si contacts implantation of single boron ions or boron monofluoride ions was considered. In contrast to phosphorus, boron is a very light atom and might penetrate the thin poly-Si films readily thereby possibly damaging the SiO_x/c-Si interface. With BF the penetration depth is reduced by 25% compared to B implantation and, more importantly, fluorine can help to passivate dangling bonds. However, the role of fluorine is ambiguous because it was found that moderate fluorine doses can have positive impacts on interface trapped charge density while higher doses can lead to defect creation in the SiO_x layer [27]. Since very high fluorine doses also dramatically increase the resistivity and/or contact resistivity of poly-Si contacts, BF_2 was abandoned after initial testing. The results show that doping by BF was more effective than doping by B for the thin poly-Si films considered here. Both B and BF implanted poly-Si contacts showed a similar dependence on doping dose as the n^+-poly-Si contacts. However, the iV_{oc} values achieved were below 700 mV, which suggests that (i) the optimum parameters have not been found yet and (ii) distinct differences between n-type and p-type poly-Si exist. Such difference in J_0 was already observed for poly-Si emitter bipolar junction transistors [28]. Possible explanations are that fewer boron atoms are segregated in grain boundaries and, thereby, passivate less defects in the poly-Si [29], and that boron leads to enhanced defect creation in the SiO_x tunnel layer [27]. To date, only one group reported very low J_0 values as low as ~4 fA/cm² for p-type poly-Si contacts [7]. Their approach includes the use of a slightly thicker thermally grown SiO_x layer, very thick poly-Si films (> 100 nm) and heavy annealing conditions including temperatures above 1000 °C, which are used to deliberately form pinholes in the thicker tunnel oxide. Given the improved thermal stability reported for ozone-based tunnel oxides [30], the use of differently grown tunnel oxides might improve the p^+-poly-Si contacts reported in this study.

In summary, it was found for both n-type and p-type poly-Si contacts that a dose of 1×10^{15} cm^{-2} in combination with an annealing temperature of 850 °C yielded the highest iV_{oc} values for every single poly-Si thickness considered here. In future research the surface passivation on textured surfaces will be addressed as well. Since average J_0 values of about 10 fA/cm² have been reported for 20 nm thin n-type TOPCon [30] and 200 nm thick n-type poly-Si contacts [31] on textured surfaces, it seems plausible that the same level of surface passivation is attainable by these n-type poly-Si contacts. However, low J_0 values for p-type passivated contacts have not been reported so far and demand a more thorough investigation.

5. Solar cells

The applicability of the poly-Si contacts as electron and hole selective contacts was investigated on simple solar cells featuring n^+-poly-Si as top contact and p^+-poly-Si as rear contact. The thickness of the poly-Si passivated contacts was varied between 6 nm, 15 nm, and 34 nm. The mean values of the single solar cell parameters are depicted in Fig. 7.

The group of solar cells featuring ~6 nm thick poly-Si contacts yielded very low V_{oc} values less than 500 mV and *FF* values not higher than 70%. Their SunsVoc characteristics exhibited already in the vicinity of 1 sun a negative slope towards lower V_{oc} values revealing a pronounced Schottky energy barrier [32]. Therefore, the pseudo *FF* (*pFF*) values could not be extracted from these measurements. This poor performance can be ascribed with the degradation of the p^+-poly-Si contact during back-end processing. This adverse effect was also observed in Ref. [33] and might be explained by the consumption of poly-Si due to weak oxidation and HF dipping (cf. Fig. 8: pronounced degradation of red response). On the other hand, the solar cells featuring 15 nm and 34 nm poly-Si films achieved quite high V_{oc} and *FF* values. The solar cells with 34 nm thick poly-Si contacts showed slightly higher V_{oc} values than those with 15 nm thick poly-Si contacts. In addition, the V_{oc} of the cells, where the p^+-poly-Si contacts were realized by B implantation, were about 10 mV lower than those with BF implantation. The V_{oc} values of all cells were in the range of 695–710 mV and limited by the inferior surface passivation properties of the p^+-poly-Si contacts. Therefore, the highest V_{oc} of 709 mV was achieved by BF implantation into 34 nm poly-Si. This is in good agreement with the results presented in Section 4, where the lowest J_0 values for both n-type and p-type poly-Si contacts were measured for the thickest films. For the cells with 15 nm and 34 nm thick poly-Si layers, there was a clear difference in V_{oc} between B and BF implantation. However, the *FF* values were similar indicating that the fluorine does not alter the transport properties of the selective hole contact system. In contrast to the trend in V_{oc}, the *FF* of the cells with 34 nm poly-Si contacts was reduced (BF doping:80.6/B doping:80.8%) compared to the cells with 15 nm poly-Si contacts (81.4/81.3%). This difference is partly due to a lower *pFF* value of 83.2% (compared to 83.6%) and partly due to a higher series resistance of 0.65 Ωcm² (compared to 0.55 Ωcm²). Please note, that the *pFF* values were about 1% lower than the implied *FF* measured by QSSPC before metallization (not shown here). This *pFF* loss can be attributed to the non-optimized solar cell structure suffering from minority carrier recombination in the peripheral region because the emitter extends to the shaded part of the wafer outside the active cell area. Due to the non-textured front and the broad metal fingers (~10% metal shading), the J_{sc} of the solar cells was basically limited to about 35 mA/cm². The cells having 15 nm poly-Si at the front exhibited a J_{sc} of about 33.4 mA/cm², while those having 34 nm poly-Si at the front achieved a lower J_{sc} of about 32.8–33.0 mA/cm².

All in all, the highest efficiency of 19.2% was achieved by the cells featuring 15 nm thick poly-Si contacts and a BF implanted p^+-poly-Si contact. The cells with 34 nm thick poly-Si films yielded a slightly lower efficiency due to lower *FF* and especially lower J_{sc} values. Moreover, the efficiency of the cells with B-implanted poly-Si contacts was slightly lower compared to those with BF-implanted poly-Si contacts due to the difference in surface passivation.

Fig. 8 depicts the internal and external quantum efficiency as well as the reflection curve measured on solar cells featuring ~6 nm, 15 nm, or 34 nm thick poly-Si films. Since the reflection curves were very similar, the IQE of the different cells can be compared directly. In the short wavelength range all cells exhibit significant current losses due to parasitic absorption in the TCO stack and the poly-Si film. It can be stated, the thicker the poly-Si, the stronger the parasitic absorption. The J_{sc} losses at the front are determined by integrating over the difference between (1-*R*)-curve and EQE weighted with the solar spectrum $AM_{1.5\,G}$ (300–700 nm). The losses amount to about 0.86, 1.0, and 1.54 mA/cm² for about 6 nm, 15 nm, and 34 nm poly-Si, respectively. These absorption losses are plotted in Fig. 9 over the poly-Si thickness. Furthermore, theoretical absorption losses for stacks of 75 nm ITO and a-Si:H (i), P-doped poly-Si, and c-Si are given. Those were calculated by OPAL [34] using the n and k data determined in Section 3 and the

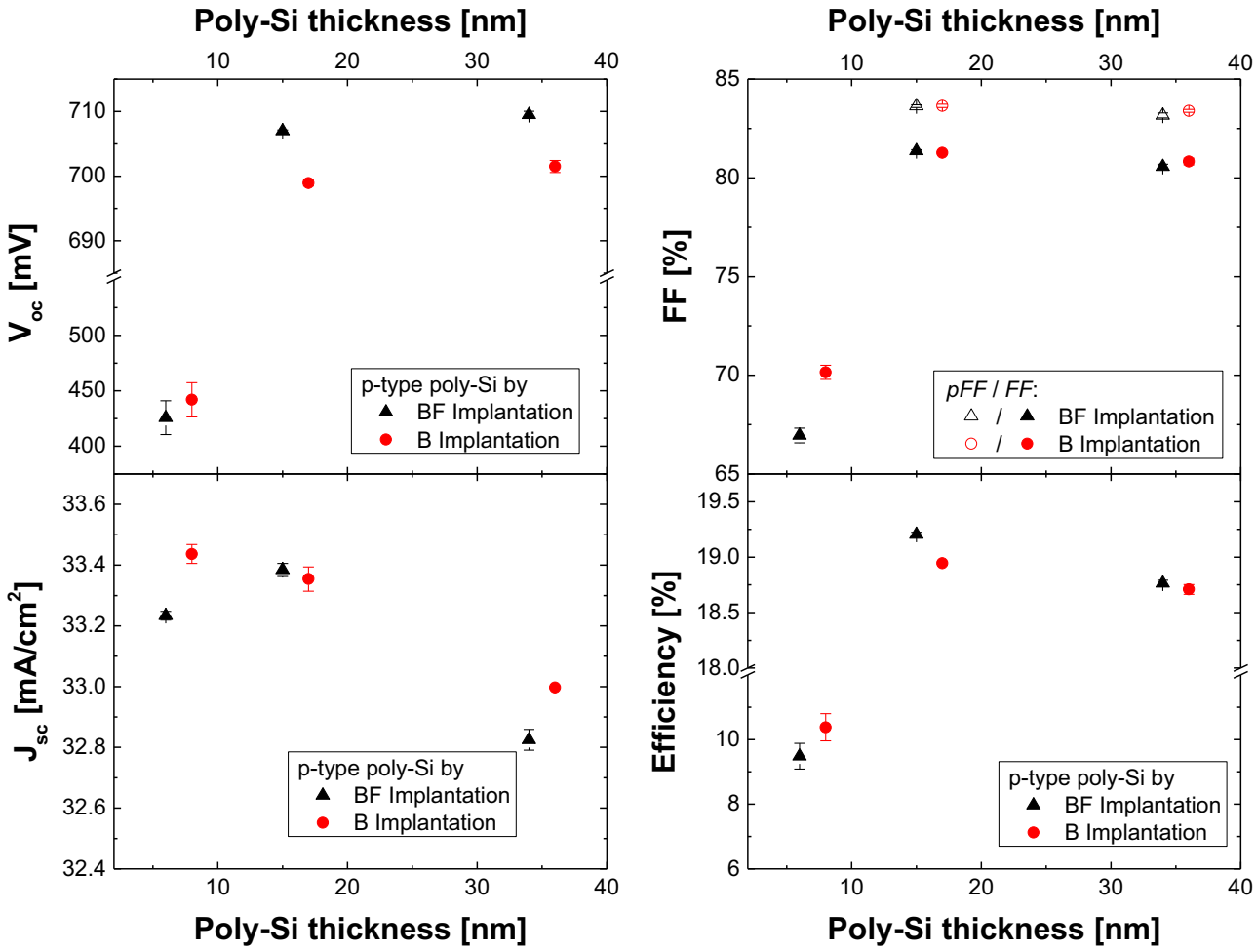

Fig. 7. Mean solar cell parameters of 7 2 × 2 cm^2 p-type solar cells featuring n-type and p-type poly-Si contacts as top/rear contacts. The p+-poly-Si contacts were either realized by implantation of BF (black symbols) or B (red symbols; placed adjacently for clarity). (For interpretation of the references to color in this figure legend, the reader is referred to the web version of this article.)

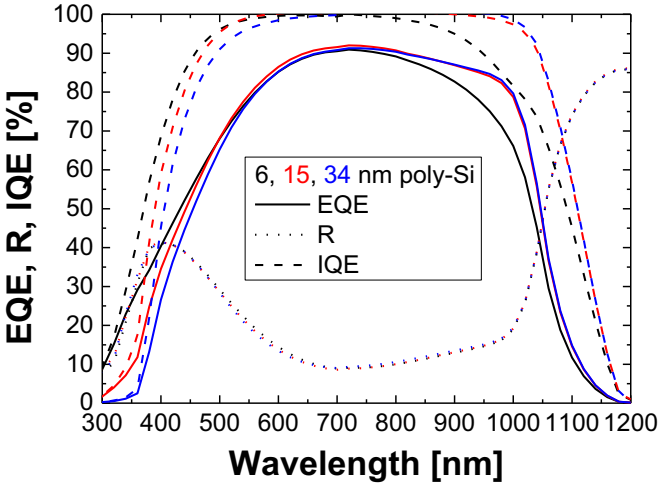

Fig. 8. External quantum efficiency (EQE), reflection (R), and internal quantum efficiency (IQE) of the solar cells with ~6 nm, 15 nm, and 34 nm poly-Si top/rear contacts. The EQE was measured after metallization.

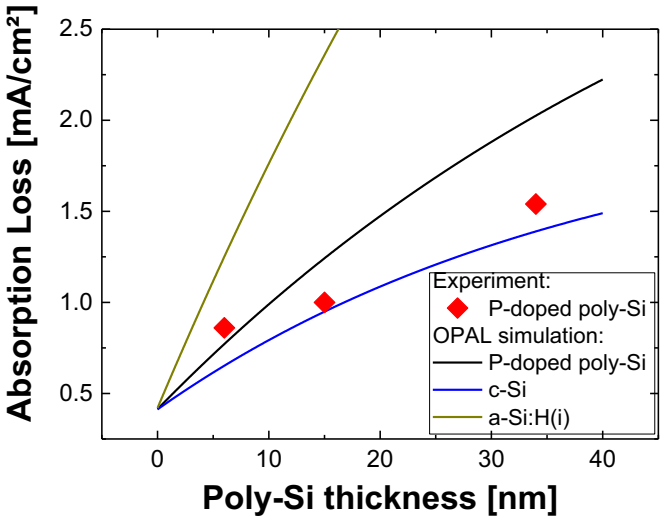

Fig. 9. Quantified absorption loss of n-type poly-Si contacts (including 75 nm TCO) vs. poly-Si film thickness. Moreover, the theoretical absorption losses in P-doped poly-Si, c-Si, and a-Si:H (i) simulated by OPAL using the n and k data of Section 3 are given.

following settings: planar surface, 200 μm thick substrate, enhancement factor Z=6. One can readily see that the experimentally determined J_{sc} loss in the 15 nm and 34 nm thin poly-Si films deviates from the theoretical curve of P-doped poly-Si and is closer to the theoretical curve of c-Si. On the other hand, the parasitic absorption losses in ~6 nm poly-Si lie above the theoretical curves. Possible reasons for this deviation could be that (i) there is a certain error in the modeled n and k data of poly-Si and (ii) a small error in the experimental data (both poly-Si thickness and measured

absorption loss). By assuming an absorption loss of ~0.4 mA/cm^2 in the TCO layer stack, the upper bound for the absorption loss in P-doped poly-Si is about 0.5 mA/cm^2 per 10 nm poly-Si. This value is still significantly lower than the J_{sc} loss in a-Si:H (1.0–1.5 mA/cm^2 per 10 nm a-Si:H [35]).

In the long wavelength range, the solar cell with 10 nm poly-Si contact showed a strong decline in EQE starting from 800 nm. This can be attributed to a degraded surface passivation of the p^+-poly-Si contacts after HF-dip. The solar cells with thicker poly-Si contacts did not show such degradation in EQE and resembled each other. The losses due to free carrier absorption (FCA) in the poly-Si layers cannot be determined unambiguously since the front is not sufficiently transparent.

6. Summary

Poly-Si/SiO_x contacts formed by LPCVD deposition of a-Si and doping via ion implantation were demonstrated. Very low J_0 values were obtained for n-type poly-Si contacts, while the p-type poly-Si contacts showed at least five times higher J_0 values. Moreover, doping of the latter by boron monofluoride helped to improve the surface passivation slightly compared to doping by boron implantation. The significant difference in surface passivation between n-type and p-type poly-Si contacts was also observed by others; however, the underlying physical mechanisms are still under discussion. Moreover, the simple solar cells with top/rear poly-Si contacts showed that these contacts are effective carrier-selective contacts thereby enabling V_{oc} values up to 709 mV and $FF > 81\%$. Finally, the solar cells and OPAL simulations show clearly that parasitic absorption in the poly-Si films is less pronounced than in a-Si:H films. Although, a solar cell with poly-Si/SiO_x contacts on both sides shares one advantage with a heterojunction solar cell, which is the higher V_{oc} than conventional diffused solar cells, it might not be an attractive alternative to a heterojunction or conventional solar cell for the following reasons: (i) the sheet resistance of very thin poly-Si films is too high to omit a TCO and (ii) although thicker poly-Si films might permit the use of SiN_x instead of a TCO, the maximum J_{sc} would be less than 40 mA/cm^2. Therefore, a more promising route for poly-Si/SiO_x contacts is their implementation into an IBC solar cell.

Acknowledgment

The authors would like to thank A. Leimenstoll, F. Schätzle, S. Seitz, N. Brändlin, and A. Lösel for sample preparation as well as E. Schäffer for measuring the solar cells. The LPCVD deposition done by M. Bauer at the institute for microsystems engineering in Freiburg is greatly acknowledged. This work was funded by the German Federal Ministry for the Economy and Energy under Grant no. 0325292 “ForTeS” and 0325827B “26+”.

References

[1] M. Taguchi, A. Yano, S. Tohoda, K. Matsuyama, Y. Nakamura, T. Nishiwaki, K. Fujita, E. Maruyama, in: Proceedings of the 39th IEEE Photovoltaic Specialists Conference, Tampa, Florida, USA, 2013.
[2] E. Yablonovitch, T. Gmitter, R.M. Swanson, Y.H. Kwark, Appl. Phys. Lett. 47 (1985) 1211.
[3] F. Feldmann, M. Bivour, C. Reichel, M. Hermle, S.W. Glunz, Sol. Energy Mater. Sol. Cells 120 (2014) 270.
[4] S.W. Glunz, F. Feldmann, A. Richter, M. Bivour, C. Reichel, H. Steinkemper, J. Benick, M. Hermle, in: Proceedings of the 31st European Photovoltaic Solar Energy Conference and Exhibition, Hamburg, 2015.
[5] D. Adachi, J.L. Hernandez, K. Yamamoto, Appl. Phys. Lett. 107 (2015).
[6] K. Masuko, M. Shigematsu, T. Hashiguchi, D. Fujishima, M. Kai, N. Yoshimura, T. Yamaguchi, Y. Ichihashi, T. Mishima, N. Matsubara, T. Yamanishi, T. Takahama, M. Taguchi, E. Maruyama, S. Okamoto, IEEE J. Photovolt. 4 (2014) 1433.
[7] U. Römer, R. Peibst, T. Ohrdes, B. Lim, J. Krugener, T. Wietler, R. Brendel, IEEE J. Photovolt. 5 (2015) 507.
[8] F. Feldmann, R. Müller, C. Reichel, M. Hermle, Phys. Status Solidi - Rapid Res. Lett. 08 (2014) 767.
[9] C. Reichel, F. Feldmann, R. Muller, R.C. Reedy, B.G. Lee, D.L. Young, P. Stradins, M. Hermle, S.W. Glunz, J. Appl. Phys. 118 (2015).
[10] G. Yang, A. Ingenito, N. van Hameren, O. Isabella, M. Zeman, Appl. Phys. Lett. 108 (2016) 033903.
[11] M. Rienäcker, A. Merkle, U. Römer, H. Kohlenberg, J. Krügener, R. Brendel, R. Peibst, in: Proceedings of the 6th International Conference on Silicon Photovoltaics, SiliconPV 2016, Chambéry, 2016.
[12] S. Lindekugel, H. Lautenschlager, T. Ruof, S. Reber, in: Proceedings of the 23rd European Photovoltaic Solar Energy Conference, Valencia, Spain, 2008, pp. 2232.
[13] R.A. Sinton, A. Cuevas, M. Stuckings, in Proceedings of the 25th IEEE Photovoltaic Specialists Conference, IEEE; New York, NY, USA, Washington DC, USA, 1996, pp. 457.
[14] F. Feldmann, K.U. Ritzau, M. Bivour, A. Moldovan, S. Modi, J. Temmler, M. Hermle, S.W. Glunz in: Proceedings of the 5th International Conference on Silicon Photovoltaics, Siliconpv, 77, 2015, pp. 263.
[15] R.A. Sinton, A. Cuevas, Proceedings of the 16th European Photovoltaic Solar Energy Conference, in: H. Scheer, B. McNelis, W. Palz, H.A. Ossenbrink, P. Helm (Eds.), James & James, Glasgow, London, UK, 2000, p. 1152.
[16] D. Pysch, A. Mette, S.W. Glunz, Sol. Energy Mater. Sol. Cells 91 (2007) 1698.
[17] G.E. Jellison, F.A. Modine, Appl. Phys. Lett. 69 (1996) 371.
[18] D.A.G. Bruggeman, Ann. Phys. 416 (1935) 636.
[19] G.E. Jellison, M.F. Chisholm, S.M. Gorbatkin, Appl. Phys. Lett. 62 (1993) 3348.
[20] H.J. Kim, C.V. Thompson, J. Electrochem. Soc. 135 (1988) 2312.
[21] D.E. Kane, R.M. Swanson, in: Proceedings of the 18th IEEE Photovoltaic Specialists Conference, Las Vegas, Nevada, USA, 1985, pp. 578.
[22] K.R. McIntosh, P.P. Altermatt, in: Proceedings of the 35th IEEE Photovoltaic Specialists Conference, 2010, pp. 2188.
[23] D. Yan, A. Cuevas, J. Bullock, Y.M. Wan, C. Samundsett, Sol. Energy Mater. Sol. Cells 142 (2015) 75.
[24] D. Yan, A. Cuevas, Y.M. Wan, J. Bullock, Sol. Energy Mater. Sol. Cells 152 (2016) 73.
[25] G.L. Patton, J.C. Bravman, J.D. Plummer, in: Proceedings of the International Electron Devices Meeting, vol. 31, 1985, pp. 30.
[26] A. Neugroschel, M. Arienzo, Y. Komem, R.D. Isaac, IEEE Trans. Electron Devices 32 (1985) 807.
[27] T. Yamamoto, K. Uwasawa, T. Mogami, IEEE Trans. Electron Devices 46 (1999) 921.
[28] C.M. Maritan, N.G. Tarr, IEEE Trans. Electron Devices 36 (1989) 1139.
[29] M.M. Mandurah, K.C. Saraswat, C.R. Helms, T.I. Kamins, J. Appl. Phys. 51 (1980) 5755.
[30] A. Moldovan, F. Feldmann, M. Zimmer, J. Rentsch, J. Benick, M. Hermle, Sol. Energy Mater. Sol. Cells 142 (2015) 123.
[31] M. Stodolny, M. Lenes, Y. Wu, G.J. M. Jansen, I.G. Romijn, J.R. M. Luchies, L.J. Geerligs, in: Proceedings of the 6th International Conference on Silicon Photovoltaics, SiliconPV 2016, 2016.
[32] M. Bivour, M. Reusch, S. Schroer, F. Feldmann, J. Temmler, H. Steinkemper, M. Hermle, IEEE J. Photovolt. 4 (2014) 566.
[33] A.D. Upadhyaya, O. Young Woo, E. Chang, V. Upadhyaya, K. Madani, K. Tate, C. Eunhwan, B. Rounsaville, V. Chandrasekaran, V. Yelundur, A. Gupta, A. Rohatgi, in: Proceedings of the IEEE 42nd Photovoltaic Specialist Conference (PVSC), 2015, pp. 1.
[34] S.C. Baker-Finch, K.R. McIntosh, in: Proceedings of the 35th IEEE Photovoltaic Specialists Conference, Honolulu, HI, USA, 2010, pp. 002184.
[35] Z.C. Holman, A. Descoeudres, L. Barraud, F.Z. Fernandez, J.P. Seif, S. De Wolf, C. Ballif, IEEE J. Photovolt. 2 (2012) 7.